Behavioral Modeling for Analog System-Level Simulation by Wavelet Collocation Method

Xin Li, Xuan Zeng, *Member, IEEE*, Dian Zhou, Xieting Ling, and Wei Cai

***Abstract*—In this paper, we propose a wavelet collocation method with nonlinear companding to generate behavioral models for analog circuits at the system level. During the overall process of circuit modeling, nonlinear function approximation is an important issue to accurately capture the nonideal input–output relations of analog circuit blocks. While a great number of previous research works focus on the high-dimensional top-down design/synthesis model, which involves large analog design spaces, this paper primarily concentrates on the bottom-up verification model requiring both simple representation and high accuracy. Taking advantage of the local support of wavelet bases, a nonlinear companding method is developed to control the modeling error distribution based on system-level simulation requirements. It, in turn, significantly improves the simulation efficiency at the system level. To demonstrate the promising features of the proposed method, two circuit examples, a fourth-order switched-current filter and a voltage-controlled oscillator, are employed to build the behavioral models.**

***Index Terms*—Analog circuits, behavioral modeling, nonlinear companding, wavelet collocation method.**

I. Introduction

With the remarkable evolution of VLSI technology, the complexity of electronic systems, including both digital and analog circuits, has increased significantly during the past twenty years. Nowadays, a great number of computations originally carried out in the analog domain are moved to their digital counterparts. However, many analog circuits, especially those for interfacing purpose such as analog-to-digital (A/D) and digital-to analog (D/A) converters, are still widely used since the real world is analog. In addition, numerous of new analog applications, such as radio frequency components, switched-current circuits, log-domain filters, and so forth, continue to appear to meet the specific requirements on circuit speed and power consumption.

As analog ICs have rapidly evolved from the relatively low complexity of the early days to the high sophistication of today, the need for more advanced behavioral modeling techniques has become increasingly urgent. First, in top-down design, quick exploration of system architectures should be carried out before detailed circuit implementation. System-level simulation based on behavioral models can provide fast prediction of system performance, which helps to select proper architectures for circuit implementation and analyze tradeoffs at the early design stages. Second, in bottom-up verification, the overall system specifications should be checked after individual circuit blocks are available. However, transistor-level simulation is too expensive in memory space and computation time to afford the verification of a whole chip containing a large number of analog components. Under such circumstance, behavioral models are extracted for each circuit block and simulated at the system level, providing the necessary information for verifying system performance.

During the past decade, various methodologies have been proposed for behavioral modeling of analog circuits. First, for linear systems, there have been a significant body of works originally evolved from the model order reduction problem for interconnect analysis [1]–[4]. These methods are mathematically elegant and are capable of generating reduced-order transfer functions for complicated linear dynamic circuits. Unfortunately, in the community of nonlinear circuit modeling, no such mature techniques exist, although several theoretical works have been developed in recent years [5]–[7]. Most practical approaches for nonlinear circuit modeling can be classified into three categories. First, the regression models proposed in [8]–[10] map the design space to the performance space directly. These methods construct high-dimensional nonlinear functions to approximate the relation between circuit performances (e.g., gain, area, dominant pole) and design parameters (e.g., transistor size). Second, for nonlinear continuous-time systems, Hammerstein model is described in [11] to separate the nonlinearity and frequency-dependency, i.e., the input–output behavior of a nonlinear dynamic circuit is approximated as a static nonlinear function followed by a linear transfer function. Finally, for switching circuits such as switched-capacitor/current filters and delta-sigma converters, the sampled-data operation can be efficiently modeled by a discrete-time system which consists of a number of ideal unit delay blocks and static nonlinear functions [12]–[14]. Clearly, for all these techniques, nonlinear function approximation is a crucial issue within the overall behavioral modeling procedure.

Manuscript received February 28, 2001; revised March 14, 2003. This work was supported in part by the National Science Foundation of China (NSFC) under Grant 69806004, Grant 69928402, Grant 60176017, Grant 60076014, and Grant 90207002, in part by National 863 plan projects of China under Grant 2002AA1Z1340 and Grant 2002AA1Z1460, in part by the Doctoral Program Foundation of Ministry of Education of China under Grant 2000024628, in part by Science & Technology Key Project of Ministry of Education of China under Grant 02095, in part by Cross-Century Outstanding Schoolars Fund of Ministry of Education of China, in part by Shanghai Science and Technology Committee Project under Grant 01JC14014, in part by Shanghai AM R&D Fund under Grant 0107 and in part by National Science Foundation under Grant NSF-0098275, Grant CCR-9972251, Grant CCR-9988375, and Grant CCR-0098140. This paper was recommended by Associate Editor H. Graeb.

X. Li, X. Zeng, and X. Ling are with the ASIC & System State Key Lab, Microelectronics Department, Fudan University, Shanghai 200433, China (e-mail: xinli@ece.cmu.edu).

D. Zhou is with the Department of Electrical and Computer Engineering, University of Texas at Dallas, Richardson, TX 75083 USA.

W. Cai is with the Department of Mathematics, University of North Carolina at Charlotte, Charlotte, NC 28233 USA.

Digital Object Identifier 10.1109/TCSII.2003.812917

There exist two approaches to approximate the nonlinear functions encountered in analog circuit modeling: 1) developing the nonlinear function manually by hand analysis [13] and 2) constructing the nonlinear approximation by data fitting [8]–[10], [12]. The first approach takes into account the internal nonidealities of analog circuits and helps designers to understand the physical behavior more accurately and intuitively. However, such a modeling method is restricted to simple circuit structures and device models. It is awkward, if not impossible, to manually extract the nonlinearity for complex circuits with sophisticated device models (e.g., BSIM3 model). Compared with the first modeling approach, the second one is more efficient and flexible. Recently, several new methodologies, including radial basis approximation [8], [9] and data mining [10], etc., have been developed to efficiently approximate the high-dimensional nonlinear functions for analog circuit modeling. These techniques mainly focus on the problem of top-down design/synthesis, where the dimension of analog design space, i.e., the number of free variables, is extremely large.

The work of this paper, on the other hand, primarily concentrates on the bottom-up verification problem. After individual circuit blocks are available, the analog design space has already been fixed and, consequently, we don't face the high-dimensional function approximation in bottom-up verification, as is the case for top-down design. The most challenging task involved here is how to accurately characterize the nonideal input-output relation with simple model representation. An accurate and simple behavioral model is crucial for bottom-up verification, because a complicated analog/mixed-signal system consisting of a great number of circuit blocks should be simulated with sufficient accuracy and acceptable computation time as well as small memory consumption. While there is a general tradeoff between modeling accuracy and model complexity, controlling error distribution of the behavioral model is an effective way to improve the overall simulation efficiency and, in the meantime, to save memory space. Namely, if the behavioral modeling error is equalized and minimized based on system-level simulation requirement, the simulation efficiency can be significantly improved.

In this paper, we propose a wavelet collocation method with nonlinear companding to address this error distribution control problem, which has been insufficiently studied in previous research works. Wavelet methods have originally been developed for imaging compression and signal decomposition [15]–[17], and later been employed to compress the integral operator encountered in electromagnetics computations [18]–[20]. The work in [21], [22] is the first one to apply the wavelet collocation method to circuit simulation. That work is extended to behavioral modeling of analog circuits in [23]. The purpose of this paper is to further develop and study the behavioral modeling problem using the spline wavelet collocation method proposed in [24].

The rest of this paper is organized as follows. In Section II, we illustrate the importance of error distribution control in behavioral modeling by an example of the switched-current memory cell. In Section III, we review the background for wavelet approximation theory, then introduce the basic principle of the wavelet collocation method for behavioral modeling in Section IV. A nonlinear companding algorithm for error distribution control is developed in Section V. To demonstrate the computational efficiency of the proposed method, two circuit examples, a fourth-order switched-current filter and a voltage-controlled oscillator (VCO), are employed in Section VI to construct the behavioral models. Finally, we draw conclusions in Section VII.

II. Importance of Error Distribution Control

The motivation for error distribution control in behavioral modeling can be illustrated by a simple example of the switched-current memory cell. For switching circuits, a high-speed clock is used to sample the input signal and convert the continuous-time signal into its discrete-time counterpart. The general purpose circuit simulators such as SPICE will spend a large amount of computation time in analyzing the transient behavior during each clock switching, resulting in expensive simulation cost for switching networks. A well-known technique for analyzing switching circuit is to model the sampled-data operation by a discrete-time system, because only the steady-state behavior at the end of each clock phase is of great interest to circuit designers.

For example, shown in Fig. 1 is the circuit schematic for a basic switched-current memory cell and its discrete-time system model. The current memory cell works in two nonoverlapping clock phases Φ_1 and Φ_2. The memory transistor M (shown in Fig. 1) sinks the input current $I_{\rm in}(t)$ during phase Φ_1 from time point $(n-1)$ to $(n-1/2)$, memories the current $I_{\rm in}(n-1/2)$, and conducts it to the output $I_{\rm out}(t)$ during phase Φ_2 from time point $(n-1/2)$ to n. It is worth noticing that the circuit state at each phase depends on the nonidealities such as charge injection, mismatch and finite input/output conductance [13], [25]. Moreover, the state of the circuit could be settled to a steady-state value during each phase switching, and the transition behavior, which may be ringing or slewing, is not important. Only the final current level at the end of each clock phase will affect the future response of the circuit. However, this current level, for example $I_{\rm out}(n)$, tends to be different from the ideal value of $I_{\rm in}(n-1/2)$ as a result of the comprehensive effect of all nonidealities. The modeling objective here is to model each current memory cell in the presence of those nonidealities using sampled data points for different input values, as expressed by (1)

$$I_{\rm out}(n)=\begin{cases} f\left[I_{\rm in}\left(n-\frac{1}{2}\right)\right], & \text{when } \Phi_2=\text{high} \\ 0, & \text{when } \Phi_2=\text{low.}\end{cases} \tag{1}$$

Function $f(\bullet)$ in (1) [also shown in Fig. 1(b)] describes the nonlinearity of the switched-current memory cell. As shown in Fig. 2, $f(\bullet)$ is very simple in this example. However, a simple $f(\bullet)$ helps us to make a full comparison between various approximation methods, and, therefore, it is a good example to be studied here.

In order to illustrate the importance of error distribution control, we approximate the nonlinear function $f(\bullet)$ (Fig. 2) in interval $[-50\,\mu\text{A}, 50\,\mu\text{A}]$ by both polynomial and spline bases, which are the most widely used basis functions in analog circuit modeling [12], [13]. For each approximation method,

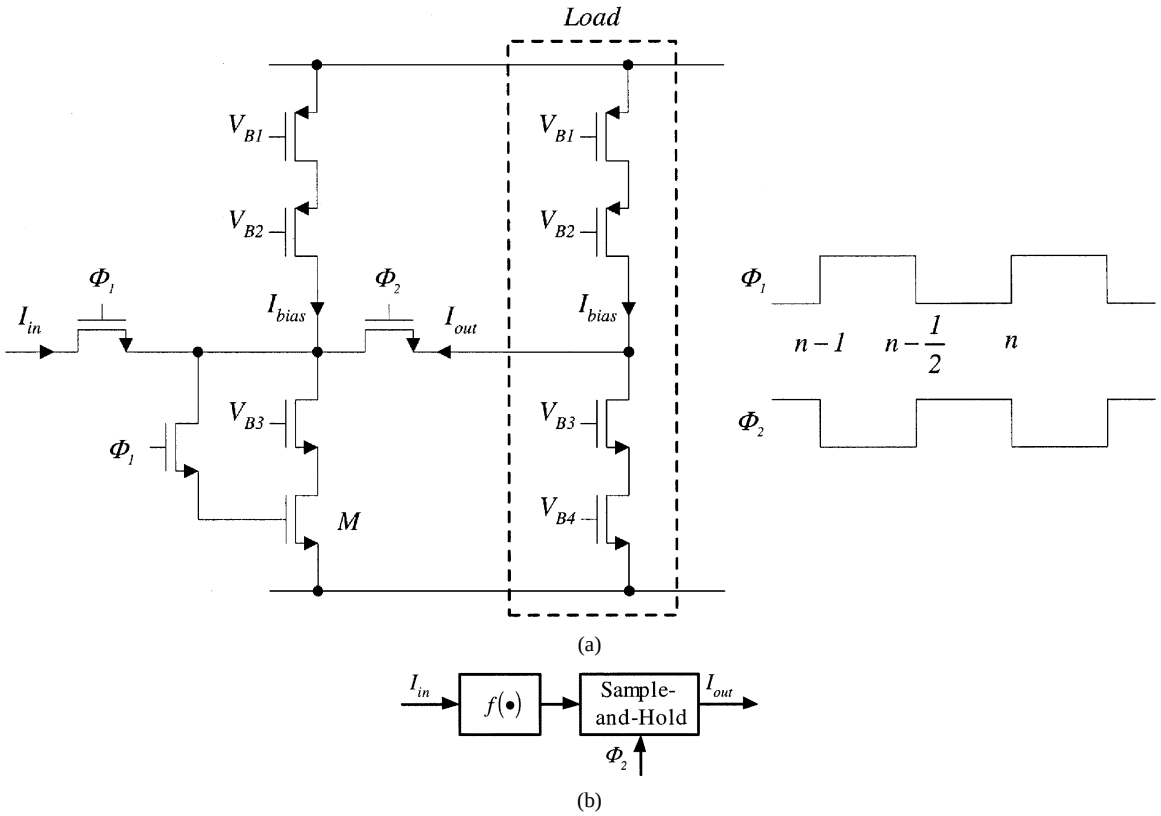

Fig. 1. A switched-current memory cell. (a) Circuit schematic for a switched-current memory cell. (b) Discrete-time system model for the switched-current memory cell.

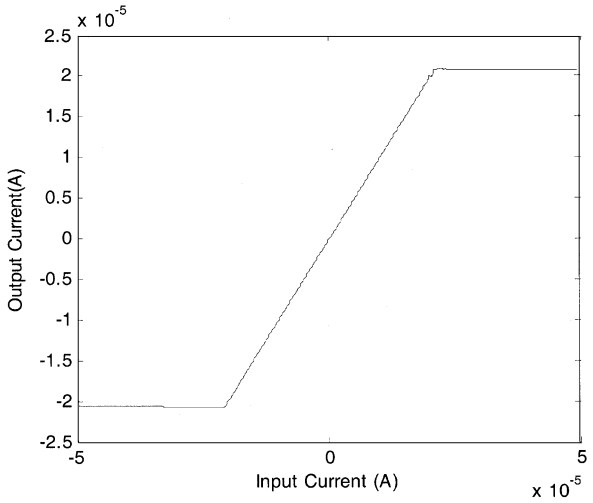

Fig. 2. Nonlinear function $f(\bullet)$ for the switched-current memory cell by SPICE.

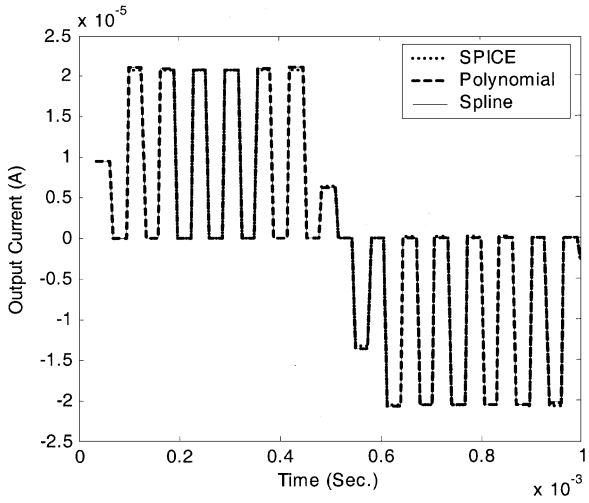

Fig. 3. Simulation result by SPICE and behavioral model with sinusoidal input $\pm 50\ \mu$A.

15 basis functions are respectively employed and the unknown coefficients for these basis functions are obtained through the least-square error approach [27]. Then, given a sinusoidal input of amplitude $\pm 50\ \mu$A (large signal input), we simulate the switched-current memory cell using these two models and reach the results in Fig. 3. Note that, the behavioral simulation is quite accurate for large signal input. Now, we decrease the sinusoidal input amplitude to $\pm 5\ \mu$A (small signal input) and re-simulate the memory cell, resulting in the output response in Fig. 4. Comparing Fig. 3 with Fig. 4, one would find that the behavioral model constructed by either polynomial or spline approximation cannot predict the circuit behavior under small signal input accurately. Table I summarizes the simulation error for various sinusoidal input amplitudes. The absolute error in Table I is defined as

$$Err_A = \sqrt{\frac{\int_0^T \left[y_{\mathrm{SPICE}}(t) - y_{\mathrm{Model}}(t)\right]^2 dt}{T}} \qquad (2)$$

where $y_{\mathrm{SPICE}}(t)$ is the simulation result by SPICE, $y_{\mathrm{Model}}(t)$ is the result by the behavioral model, and $[0, T]$ is the overall

TABLE I
SIMULATION RESULT FOR THE SWITCHED-CURRENT MEMORY CELL

Input signal amplitude	Absolute error		Relative error	
	Polynomial	Spline	Polynomial	Spline
$\pm 5\mu A$ (small signal input)	1.66×10^{-7}	1.06×10^{-7}	6.64%	4.26%
$\pm 20\mu A$	2.12×10^{-7}	2.07×10^{-7}	2.12%	2.07%
$\pm 35\mu A$	1.62×10^{-7}	1.81×10^{-7}	1.29%	1.43%
$\pm 50\mu A$ (large signal input)	1.55×10^{-7}	1.70×10^{-7}	1.15%	1.27%

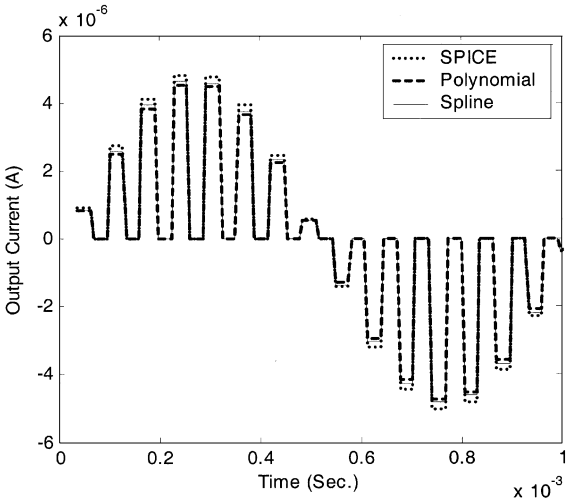

Fig. 4. Simulation result by SPICE and behavioral model with sinusoidal input $\pm 5\ \mu$A.

simulation interval in time domain. Similarly, the relative error is defined as

$$Err_R = \sqrt{\frac{\int_0^T \left[y_{\rm SPICE}(t) - y_{\rm Model}(t)\right]^2 dt}{\int_0^T \left[y_{\rm SPICE}(t)\right]^2 dt}}. \tag{3}$$

A close studying on Table I indicates that the absolute modeling errors for various sinusoidal input amplitudes are almost identical. However, the relative modeling errors for small signal input are about three to six times as those for large signal input. This simple example demonstrates two important issues in behavioral modeling.

a) The behavioral model developed by conventional polynomial or spline approximation cannot achieve the same accuracy for various input/output amplitudes.
b) As a criterion for system-level simulation, the relative error is stricter than the absolute one in evaluating the accuracy of behavioral models. Therefore, it is more desirable to keep the relative modeling error being uniformly distributed over various circuit input/output values.

The above two observations motivate us to propose the wavelet approximation with nonlinear companding for error distribution control in behavioral modeling, which will be presented in detail in Sections III–VI.

III. BACKGROUND FOR WAVELET APPROXIMATION THEORY

A. Wavelet Basis Functions

The wavelet basis functions can be constructed by many means [17], but in this paper, we will use the spline wavelets developed in [24] because they were proved to have a high convergence rate. Let $H^2[0, L]$ be the Sobolev space, which basically contains all functions with square integrable second order derivatives [26]. We first introduce the following function subspaces:

$$\begin{aligned} V_{-1} =& \\ & \operatorname{span}\left\{ \begin{matrix} \eta_1(t), \eta_2(t), \eta_1(L-t), \eta_2(L-t), \varphi_{0,-1}(t) \\ \varphi_{0,0}(t), \varphi_{0,1}(t), \ldots, \varphi_{0,L-4}(t), \varphi_{0,L-3}(L-t) \end{matrix} \right\} \\ W_J =& \\ & \operatorname{span}\left\{ \Psi_{J,K}(t)\ , -1 \le K \le 2^J - 2 \right\}, \quad J \ge 0 \\ V_J =& V_{J-1} \oplus W_J, \quad J \ge 0 \end{aligned} \tag{4}$$

where the definitions of functions $\eta_1(t)$, $\eta_2(t)$, $\varphi_{0,-1}(t)$, $\{\varphi_{0,K}(t), 0 \le K \ge L-4\}$, $\varphi_{0,L-3}(L-t)$ and $\left\{ \Psi_{J,K}(t), -1 \le K \le 2^J - 2\ ,\ J \ge 0 \right\}$ are given below. $\operatorname{span}\{f_1, f_2, \ldots, f_N\}$ is a function set formed by all linear combinations of functions $f_1, f_2, \ldots, f_N$ and $\oplus$ stands for the direct sum.

In (4), functions $\eta_1(t)$ and $\eta_2(t)$ are used to handle the nonhomogeneity of the boundary data

$$\begin{aligned} \eta_1(t) =& (1-t)_+^3 \\ \eta_2(t) =& 2t_+ - 2t_+^2 + \frac{7}{6}t_+^3 - \frac{4}{3}(t-1)_+^3 + \frac{1}{6}(t-2)_+^3 \end{aligned} \tag{5}$$

where

$$t_+^n = \begin{cases} t^n, & \text{if } t \ge 0 \\ 0, & \text{otherwise.} \end{cases} \tag{6}$$

The boundary scaling functions are

$$\begin{aligned} \varphi_{0,-1}(t) =& \varphi_b(t) = \frac{3}{2}t_+^2 - \frac{11}{12}t_+^3 + \frac{3}{2}(t-1)_+^3 \\ & - \frac{3}{4}(t-2)_+^3 + \frac{1}{6}(t-3)_+^3 \\ \varphi_{0,L-3}(t) =& \varphi_b(L-t) \end{aligned} \tag{7}$$

and the interior scaling functions are

$$\varphi_{0,K}(t) = \varphi(t-K), \quad 0 \le K \le L-4 \tag{8}$$

where

$$\begin{aligned} \varphi(t) = \frac{1}{6}t_+^3 - \frac{2}{3}(t-1)_+^3 + (t-2)_+^3 \\ - \frac{2}{3}(t-3)_+^3 + \frac{1}{6}(t-4)_+^3 \end{aligned} \tag{9}$$

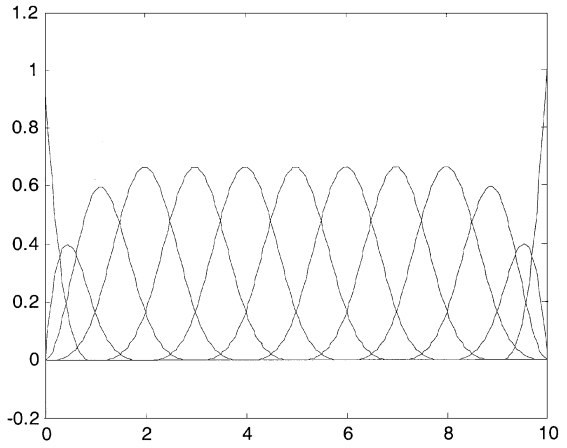

Fig. 5. Wavelet basis functions in subspace V_{-1}.

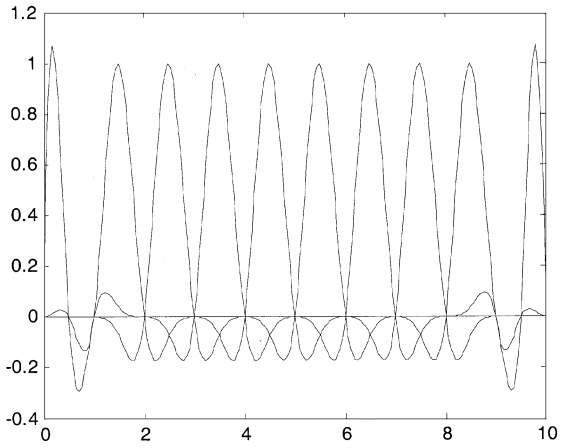

Fig. 6. Wavelet basis functions in subspace W_0.

The functions defined in (5)–(9). construct the bases of the subspace V_{-1} in (4). Fig. 5 displays those wavelet basis functions for subspace $V_{-1} \subset H^2[0, 10]$. Note that all wavelet bases are located in a finite interval, i.e., wavelet basis functions have compact support. This is the key difference between wavelet bases and other global support basis functions such as polynomial ones.

Now, consider the subspace W_J in (4). The boundary wavelet functions are

$$\begin{aligned} \psi_{j,-1}(t) =& \psi_{b0}(2^J t) \\ \psi_{J,0}(t) =& \psi_{b1}(2^J t) \\ \psi_{J,2^J-3}(t) =& \psi_{b1}\left[2^J(L-t)\right] \\ \psi_{J,2^J,-2}(t) =& \psi_{b0}\left[2^J(L-t)\right] \end{aligned} \tag{10}$$

where

$$\begin{aligned} \psi_{b0}(t) =& -\frac{56}{99}\left[14\psi(t+2)+\psi(t+1)\right] \\ \psi_{b1}(t) =& -\frac{182}{181} \\ & \times\left[\psi(t)+\frac{1}{13}\psi(t+1)+\frac{1}{13}\psi(t+2)\right] \end{aligned} \tag{11}$$

and the interior wavelet functions are

$$\psi_{J,K}(t) = \psi\left(2^J - K\right), \quad 1 \le K \le 2^J - 4 \tag{12}$$

where

$$\psi(t) = -\frac{3}{7}\varphi(2t) + \frac{12}{7}\varphi(2t-1) - \frac{3}{7}\varphi(2t-2). \tag{13}$$

The functions defined in (10)–(13). construct the bases of the subspace W_J in (4). Figs. 6 and 7 show the wavelet basis functions for subspace $W_0 \subset H^2[0,\ 10]$ and $W_1 \subset H^2[0,\ 10]$ respectively. Comparing Fig. 6 with Fig. 7, one would find that, as the wavelet subspace level J increases, high-level wavelet basis functions in subspace W_J have high order singularities. Here, singularity means the fast changing of the function waveform, which also implies the high frequency components in the frequency spectrum of the function. Therefore, as more high-level wavelet basis functions are included, the approximation error can be reduced.

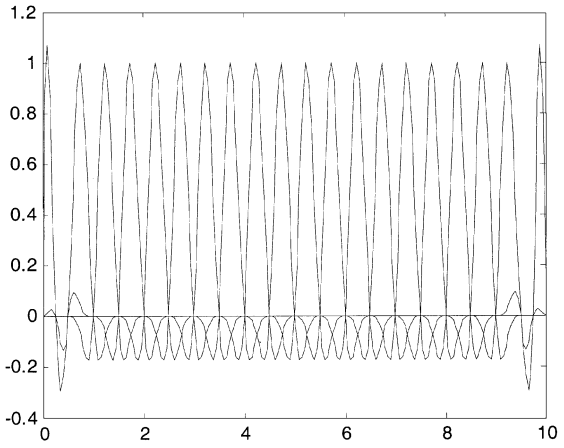

Fig. 7. Wavelet basis functions in subspace W_1.

B. Adaptive Scheme

One of the main advantages of the wavelet approximation is that there exists an adaptive scheme, which relies on the multiresolution analysis in wavelet theory [17], [22], [24]. Using the adaptive technique, those wavelet basis functions, which are needed for approximating the given nonlinear function, can be employed automatically. It, in turn, improves the approximation efficiency significantly. The spline wavelets in [24] consist of a closed subspace of $H^2[0, L]$:

$$\begin{aligned} V_J =& V_{-1} \oplus W_0 \oplus W_1 \oplus \cdots \oplus W_J \\ V_J =& V_{J-1} \oplus W_J \\ V_{-1} \subset& V_0 \subset V_1 \cdots \end{aligned} \tag{14}$$

where the notation $\oplus$ stands for the direct sum.

As illustrated in [22], [24], the magnitude of the wavelet coefficients in W_J indicates whether a refinement, by increasing the wavelet space level J, is needed or not. For example, define the maximum relative magnitude of the wavelet coefficients in W_J as

$$R_J = \frac{\operatorname{Max}\left|C_i^J\right|}{\operatorname{Max}|C_i|} \tag{15}$$

where $\operatorname{Max}\left|C_i^J\right|$ is the maximum magnitude of the wavelet coefficients in W_J, and $\operatorname{Max}|C_i|$ is the maximum magnitude of all

wavelet coefficients. If R_J is greater than a given error tolerance ε, we increase the wavelet space level J to J', where $J' > J$ [22], [24].

More importantly, because of the local support of wavelet bases, not all basis functions in higher wavelet spaces W_J are needed in order to achieve more accuracy. Actually, only basis functions, whose local positions require high accuracy, should be included [21], [22], [24]. In other words, suppose that function $f(x)$ is defined in interval $[A, B]$, then the adaptive algorithm divides the overall interval $[A, B]$ into a set of sub-intervals $[C_1, C_2], [C_2, C_3], \ldots, [C_{N-1}, C_N]$, where $C_1 = A$ and $C_N = B$. In each sub-interval, a proper wavelet space W_J is adaptively assigned for approximating f_x. Because the wavelet space level J employed in each sub-interval is different from each other, the modeling error distribution, consequently, is regulated. From this viewpoint, the wavelet approximation has the potential to control the error distribution, which is not affordable by other approximation methods with global support bases, e.g., the polynomial approach.

However, the above adaptive algorithm presents some limitations in analog circuit modeling. It is shown in (10)–(13) that the wavelet bases in W_J are generated if we compress those basis functions in lower level space W_{J-1} by one time. Consequently, the singularity of the wavelet bases in W_J is doubled, compared with that in W_{J-1}. Note that the singularity of basis functions doesn't change continuously when the wavelet space level J is increased. It, in turn, implies that the approximation error doesn't change continuously either, because the singularity of wavelet basis functions determines their capability for approximation [17], [21], [22], [24]. As a result, the modeling error cannot be regulated smoothly from one sub-interval $[C_i, C_{i+1}]$ to its neighborhood $[C_{i+1}, C_{i+2}]$ or $[C_{i-2}, C_{i-1}]$. The disclosure of the above limitation motivates us to develop a new nonlinear companding method for error distribution control, which is described detailedly in Sections IV–VI.

IV. Behavioral Modeling by Wavelets

In this section, we first develop the wavelet collocation method for approximating one-dimensional nonlinear functions, then extend the proposed method to high-dimensional functions.

A. Wavelet Approximation for One-Dimensional Functions

Without loss of generality, we assume that the nonlinear function for approximation is denoted by

$$y = f(x). \tag{16}$$

According to the wavelet approximation theory [17], function $f(\bullet)$ can be expanded by

$$y = \sum_{i=1}^{M} C_i \cdot W_i(x) \tag{17}$$

where $\{C_i; i = 1, 2, \ldots, M\}$ are unknown coefficients, $\{W_i(x); i = 1, 2, \ldots M\}$ are wavelet basis functions, and M is the total number of basis functions that have been employed.

Discretize (17) at some interior collocation points $\{x_1, x_2, \ldots, x_N; N \geq M\}$, then (17). can be written in a familiar form

$$C \cdot F = Y \tag{18}$$

where

$$C = [\, C_1 \quad C_2 \quad \cdots \quad C_M \,] \tag{19}$$

$$F = \begin{bmatrix} W_1(x_1) & W_1(x_2) & \cdots & W_1(x_N) \\ W_2(x_1) & W_2(x_2) & \cdots & W_2(x_N) \\ \vdots & \vdots & \vdots & \vdots \\ W_M(x_1) & W_M(x_2) & \cdots & W_M(x_N) \end{bmatrix} \tag{20}$$

$$Y = [\, y(x_1) \quad y(x_2) \quad \cdots \quad y(x_N) \,]. \tag{21}$$

For each value x_i, $y(x_i)$ can be found by a transistor-level simulator such as SPICE. Then, the optimal solution for (18) with least-square error is given by [27]

$$C = Y \cdot F^T \cdot \left(F \cdot F^T\right)^{-1} \tag{22}$$

where T denotes the operation of transpose.

B. Wavelet Approximation for High-Dimensional Functions

High-dimensional wavelet basis functions can be generated from tensor products of low-dimensional bases [28]. For example, if $\{W_i(x); i = 1, 2, \ldots, M\}$ are one-dimensional wavelet bases, then functions $\{W_i(x) \cdot W_j(y); i, j = 1, 2, \ldots, M\}$ construct a set of two-dimensional wavelet basis functions. In general, a K-dimensional nonlinear function with K input variables $\{x1, x2, \ldots, xK\}$

$$y = f(x1, x2, \ldots, xK) \tag{23}$$

can be expressed by wavelet expansion

$$y = \sum_{i1=1}^{M1} \sum_{i2=1}^{M2} \cdots \sum_{iK=1}^{MK} C_{i1,i2,\ldots,iK} \cdot \left[W_{i1}^1(x1) \cdot W_{i2}^2(x2) \cdots W_{iK}^K(xK)\right] \tag{24}$$

where $\{C_{i1,i2,\ldots,iK}; i1 = 1, 2, \ldots, M1; \ldots; iK = 1, 2, \ldots, MK\}$ are unknown coefficients and $\left\{W_{i1}^1(x1) \cdot W_{i2}^2(x2) \cdots W_{iK}^K(xK); ij = 1, 2, \ldots, Mj\right\}$ are K-dimensional wavelet bases [28]. Equation (24) shows that a K-variable nonlinear function is approximated by the linear combination of $M1 \cdot M2 \cdots MK$ K-dimensional wavelet basis functions. The overall number of unknown coefficients, therefore, is $M1 \cdot M2 \cdots MK$. Those unknown parameters can be obtained by a similar approach as that for one-dimensional cases, i.e., discretizing (24) at $N1 \cdot N2 \cdots NK$ $(N1 \geq M1, \ldots, NK \geq MK)$ interior collocation points $\{x1_1, x1_2, \ldots, x1_{N1}; \ldots; xK_1, xK_2, \ldots, xK_{NK}\}$ then solving the corresponding linear equation to find the least-square error solution.

It is worth mentioning that the above nonlinear function approximation scheme can be practically used when the function dimension is not very large. For bottom-up verification, which is essentially what this paper focuses on, the analog design space has already been fixed and the nonlinear function in (23) does

not include design parameters as input variables. In such cases, the dimension of the nonlinear function is small and, therefore, the expansion in (24) can be efficiently applied.

V. Error Distribution Control by Companding

In this section, we propose a nonlinear companding technique to regulate the error distribution, so that the modeling error can satisfy the system-level simulation requirement. For example, the relative error is equalized at different circuit input/output values.

A. Algorithm of Nonlinear Companding

According to the wavelet approximation theory [17], the approximation error depends on the singularity of wavelet basis functions. Singular basis functions are capable of capturing the high frequency components of $f(x)$, and thereby improve the approximation accuracy. Hence, the modeling error distribution can be modified if the singularity of wavelet bases is changed. This idea can be realized by a nonlinear companding algorithm introduced in the following.

Assume that function $f(x)$ is defined in interval $[x_A, x_B]$. We call $[x_A, x_B]$ the *Input Domain*. On the other hand, we artificially define the wavelet basis functions $\{W_i(l); i = 1, 2, \ldots, M\}$ in another domain $[l_A, l_B]$, which is called the *Companding Domain*. The relation between the *Input Domain* and the *Companding Domain* is determined by a nonlinear companding function $l = g(x)$. Now, with nonlinear companding, the original wavelet expansion in (17) is modified to

$$\begin{aligned} y = & f(x) = f\left[g^{-1}(l)\right] = \sum_{i=1}^{M} C_i \cdot W_i(l) \\ = & \sum_{i=1}^{M} C_i \cdot W_i\left[g(x)\right] \end{aligned} \tag{25}$$

where $x = g^{-1}(l)$ is the inverse function of $l = g(x)$, and wavelet coefficients $\{C_i; i = 1, 2, \ldots, M\}$ can be obtained by the collocation method illustrated in Section IV. The nonlinear function $l = g(x)$ defined in interval $[x_A, x_B]$ should satisfy the following constraints.

a) $g(x_A) = l_A = x_A$ and $g(x_B) = l_B = x_B$.
b) Function $l = g(x)$ is monotonically increasing.

Hence, function $l = g(x)$ establishes a one-to-one mapping between the *Input Domain* and the *Companding Domain*. It is worthy mentioning that these two constraints are sufficient, but not necessary, conditions for constructing a companding function. For example, a monotonically decreasing function may also be suitable for nonlinear companding. For the reason of simplicity, we only discuss those companding functions satisfying the proposed two constraints in this paper, since similar results can be reached in other cases.

The nonlinear companding algorithm discussed above can be easily extended to high-dimensional functions. Considering a function with K input variables $\{x_1, x_2, \ldots, x_K\}$, we define a set of nonlinear functions $\{l_i = g_i(x_1, x_2, \ldots, x_K); i = 1, 2, \ldots, K\}$ to establish a one-to-one mapping from the K-dimensional *Input Domain* $\{x_1, x_2, \ldots, x_K\}$ to the K-dimensional *Companding Domain* $\{l_1, l_2, \ldots, l_K\}$. Then, the principles introduced in this section can be applied straightforwardly.

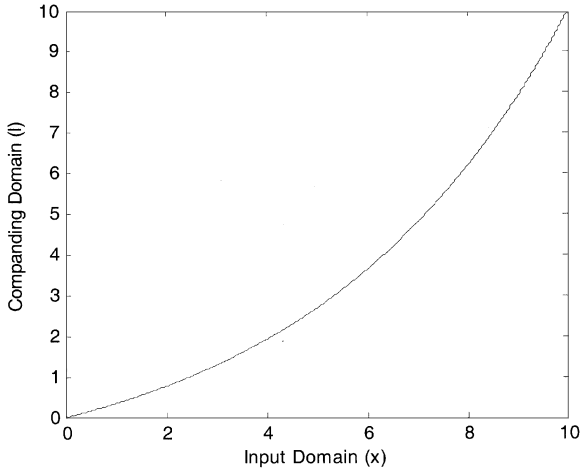

Fig. 8. Concave function for nonlinear companding.

Note that the actual basis functions, which are used to represent $f(x)$ in (25), are $\{W_i[g(x)]; i = 1, 2, \ldots, M\}$. The singularity of $W_i[g(x)]$ will be changed if $g(x)$ is modified. Therefore, by using proper companding function $l = g(x)$, we can force the modeling error distribution satisfy certain specifications required by the system-level simulation. The mechanism of the nonlinear companding for error distribution control and the method of constructing the companding functions will be presented in the following.

B. Mechanism of Nonlinear Companding

The mechanism of nonlinear companding can be illustrated either in *Input Domain* or equivalently in *Companding Domain*.

1) Analysis of Companding in Input Domain: Equation (25). implies that the process of nonlinear companding is equivalent to transforming a set of wavelet basis functions $\{W_i(l); i = 1, 2, \ldots, M\}$ initially in *Companding Domain* to their counterparts $\{W_i[g(x)]; i = 1, 2, \ldots, M\}$ in *Input Domain*. Then, the companded basis functions $W_i[g(x)]$ are employed to expand the nonlinear function $f(x)$ in *Input Domain*. The first-order derivative of $W_i[g(x)]$ is

$$\frac{dW_i}{dx} = \frac{dW_i}{dl} \cdot \frac{dl}{dx} = \frac{dW_i}{dl} \cdot g'(x); \quad i = 1, 2, \ldots, M. \tag{26}$$

Equation (26) demonstrates that the derivative of $W_i(l)$ is scaled by $g'(x)$ after nonlinear mapping. Since the derivative of a function indicates its singularity, (26) thus implies that the singularity of the original wavelet basis functions dW_i/dl is changed in *Input Domain*. For example, consider the concave function $l = g(x) = 10 \cdot (e^{0.2x} - 1)/(e^2 - 1)$ (displayed in Fig. 8), which is defined in interval $[0, 10]$. Fig. 9 gives the waveforms of a set of wavelet basis functions with uniform level in the *Companding Domain*, and their equivalent counterparts in *Input Domain* are depicted in Fig. 10. Comparing Fig. 9 with Fig. 10, one would notice that the companded wavelet basis functions near $x = 10$ have higher order singularities than that near $x = 0$. Such a feature can be explained as a result of the nonlinear mapping, because the first-order derivative $g'(x)|_{x=10} > 1$ and

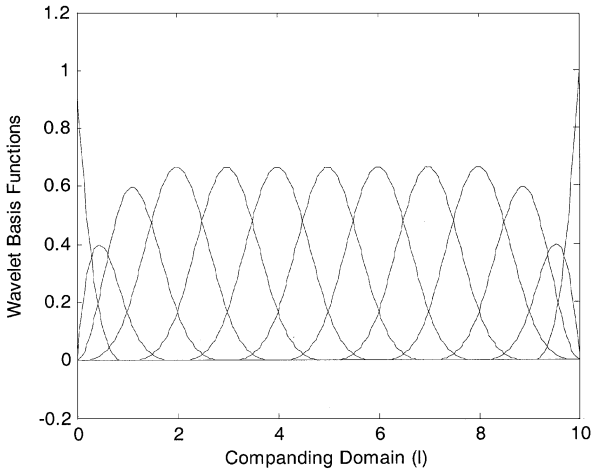

Fig. 9. Wavelet basis functions in *Companding Domain*.

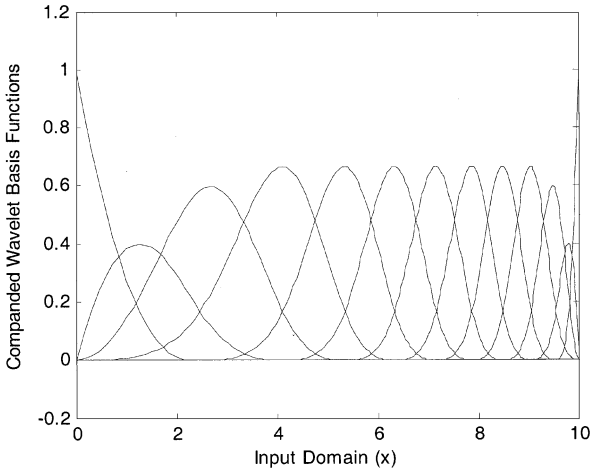

Fig. 10. Companded wavelet basis functions in *Input Domain*.

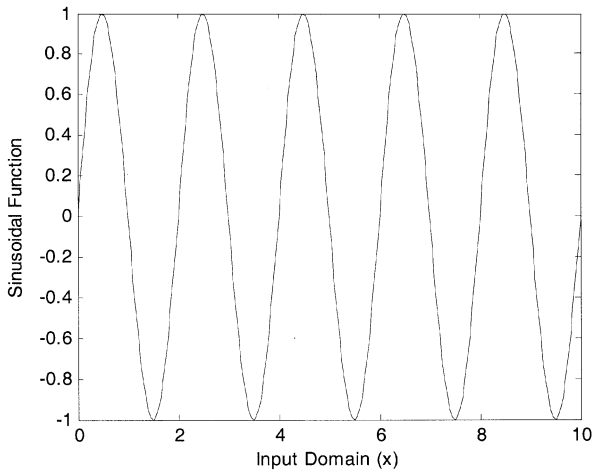

Fig. 11. Sinusoidal function in *Input Domain*.

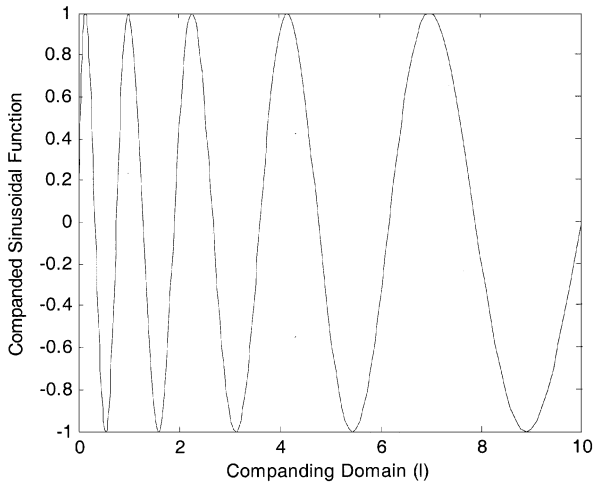

Fig. 12. Companded sinusoidal function in *Companding Domain*.

$g'(x)|_{x=0} < 1$. Therefore, when the companded wavelet basis functions are used to represent function $f(x)$ in *Input Domain*, the singular bases near $x = 10$ have the potential to approximate $f(x)$ more accurately since they contain more high frequency components.

The above analysis indicates that from the viewpoint of wavelet basis functions, the modeling error in one interval can be reduced by increasing the singularity of wavelet bases in that region. According to (26), the singularity of wavelet bases is proportional to $g'(x)$, i.e., the greater the first-order derivative $g'(x)$ is, the more singular the wavelet bases will be. Therefore, we shall increase the value of $g'(x)$ in those regions where high modeling accuracy is required.

2) Analysis of Companding in Companding Domain: Considering (25), one would find that the process of nonlinear companding is also equivalent to transforming the function $f(x)$ initially defined in *Input Domain* into its counterpart $f[g^{-1}(l)]$ in *Companding Domain*. Then, the companded function $f\left[g^{-1}(l)\right]$ is expanded by wavelets $\{W_i(l); i = 1, 2, \ldots, M\}$ in *Companding Domain*. The first-order derivative of $f[g^{-1}(l)]$ is given by

$$\frac{df}{dl} = \frac{df}{dx} \cdot \frac{dx}{dl} = \frac{df}{dx} \cdot \frac{1}{\frac{dl}{dx}} = \left.\frac{f(x)}{g(x)}\right|_{x=g^{-1}(l)}. \quad (27)$$

The above equation indicates that the derivative of $f(x)$ is scaled by $1/g'(x)$ after nonlinear mapping, and consequently, the singularity of the original function is changed in *Companding Domain*. For example, $l = g(x)$ is given in Fig. 8 and function $f(x)$ is a sinusoidal one depicted in Fig. 11. The companded sinusoidal function $f\left[g^{-1}(l)\right]$ in *Companding Domain* is displayed in Fig. 12. Note that the original function $f(x)$ has been compressed near $x = 0$ but expanded near $x = 10$. The companded function $f\left[g^{-1}(l)\right]$ then becomes increasingly singular near $l = 0$ and very smooth near $l = 10$, since the first-order derivative $1/g'(x)|_{x=0} > 1$ and $1/g'(x)|_{x=10} < 1$. As a result, when function $f\left[g^{-1}(l)\right]$ is represented by wavelet expansion with uniform level (displayed in Fig. 9), the modeling error near $l = 0$ will be greater than that near $l = 10$, because waveforms near $l = 0$ contain more high frequency components and they are more difficult to be approximated than the smooth waveforms near $l = 10$.

In summary, we can reduce the modeling error in one interval by smoothing the function $f(x)$ in that region. Equation (27) implies that the singularity of $f(x)$ is reversely proportional to $g'(x)$, i.e., the greater the first-order derivative $g'(x)$ is, the less singular the function $f(x)$ will be. Therefore, we shall increase

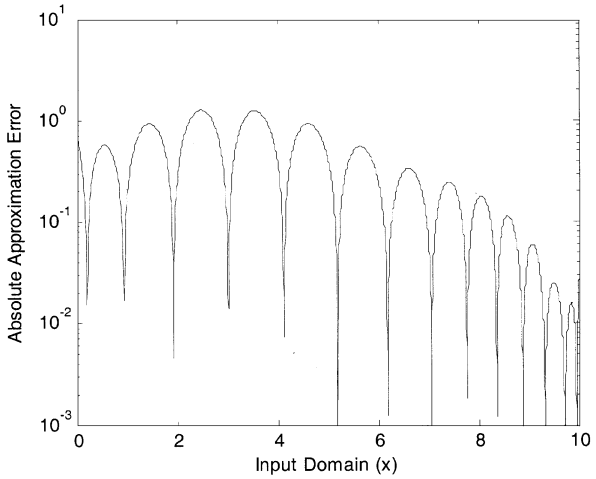

Fig. 13. Absolute approximation error by the concave function.

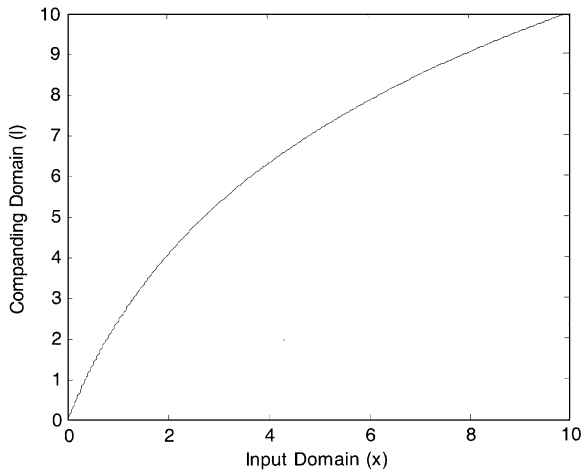

Fig. 14. Convex function for nonlinear companding.

the value of $g'(x)$ in those regions where high model accuracy is needed.

Actually, the idea of nonlinear companding is not a new one, but has already been widely used in communication [29], audio magnetic recording [30] and analog circuit design [31], [32]. Although the mechanism for those three applications and our analog circuit modeling is different, the motivation for companding is the same, i.e., to improve the signal-to-noise ratio (SNR) at small signal region with the cost of a little lose of accuracy at large signal region. Consequently, the SNR at any input/output amplitude is kept above a minimum acceptable level. In case of analog circuit modeling, we can regard the exact waveform to be approximated as signal and the approximation error as noise.

C. Constructing the Companding Function

It has been shown in Sections V-A and B that we shall increase the value of $g'(x)$ in those regions where high modeling accuracy is needed.

a) If the modeling error is required to be decreasing in interval $[A, B]$, then $g'(x)$ should be increasing in $[A, B]$. In this case, a concave function, such as the exponential function, can be chosen for companding. For example, let

$$l = g(x) = \frac{10}{e^2 - 1} \cdot \left(e^{0.2x} - 1\right) \tag{28}$$

as shown in Fig. 8. Applying nonlinear companding with such a companding function, we approximate the sinusoidal function in Fig. 11 by wavelet bases in Fig. 9. The absolute approximation error is depicted in Fig. 13. Note that the error near $x = 0$ is about 50 times as that near $x = 10$, which is consistent with our requirement.

b) Contrarily, if the modeling error is needed to be increasing in interval $[A, B]$, then $g'(x)$ should be decreasing in $[A, B]$. In this case, a convex function, such as the logarithmic function, can be chosen for companding. For example, let

$$l = g(x) = \frac{10}{\ln 7} \cdot \ln\left(1 + 0.6x\right) \tag{29}$$

as shown in Fig. 14. Applying nonlinear companding with such a companding function, we approximate the sinusoidal function in Fig. 11 by wavelet bases in Fig. 9. The absolute approximation error is depicted in Fig. 15. Now, the error near $x = 10$ is about 50 times as that near $x = 0$, as specified in our requirement.

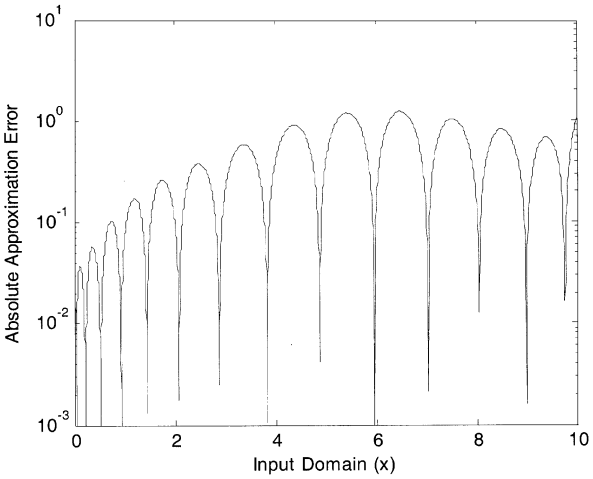

Fig. 15. Absolute approximation error by the convex function.

The concave and convex functions discussed above are two kinds of basic functions for nonlinear companding. More complicated functions can be constructed by these two basic ones. For example, if the modeling error is required to be decreasing in $[0, 5]$ and increasing in $[5, 10]$, then we can build a companding function with the combination of one concave and one convex function. Define

$$l = g(x) = \frac{5 \cdot \operatorname{sign}(x - 5)}{\ln 11} \cdot \ln\left(1 + 2\left|x - 5\right|\right) + 5 \tag{30}$$

which is depicted in Fig. 16. We approximate the sinusoidal function in Fig. 11 with such a companding function. The absolute approximation error is displayed in Fig. 17. Note that the error near $x = 5$ is only 5% of that near $x = 0$ and $x = 10$.

The above discussion has given a qualitative analysis on how to define a proper companding function $l = g(x)$ to reduce the modeling error in some specific regions. Unfortunately,

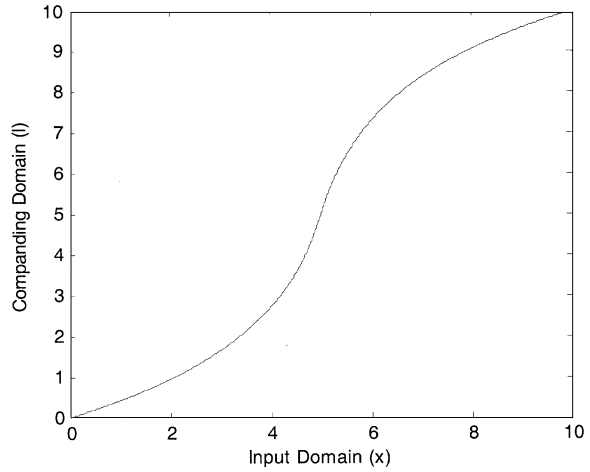

Fig. 16. The combination of one concave and one convex function for nonlinear companding.

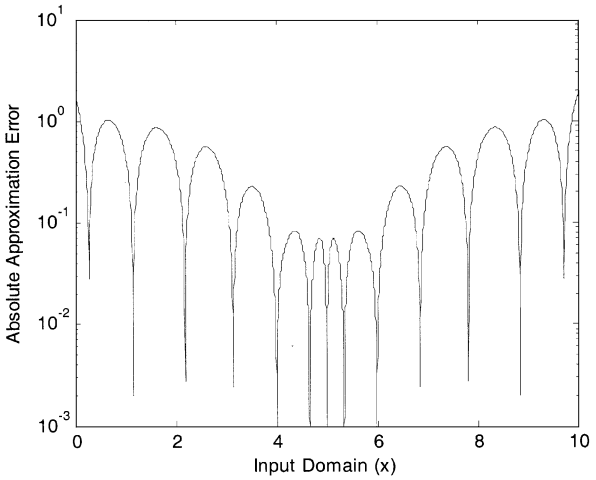

Fig. 17. Absolute approximation error by the combination of concave and convex functions.

the quantitative relation between modeling error and the companding function $l = g(x)$ is unavailable, because the exact error is determined by not only the function $l = g(x)$ but also many other factors, such as the singularity of the function to be approximated, the singularity of the wavelet basis functions that are employed, etc. In practical applications, we can build the companding function $l = g(x)$ by three steps.

Step 1) Specify the requirements on modeling error distribution. For instance, the relative simulation error is to be equalized.

Step 2) Based on those requirements developed in Step 1, determine the prototype of the companding function, i.e., whether concave function, convex function or their combination should be used.

Step 3) Refine the prototype of $l = g(x)$ repeatedly, so that the exact modeling error meets those requirements given in Step 1.

Step 3 can be carried out automatically by an optimization process, if the modeling requirements are mathematically expressed as an explicit merit function. In Section VI, we will show how to construct proper companding functions step by step in two circuit examples.

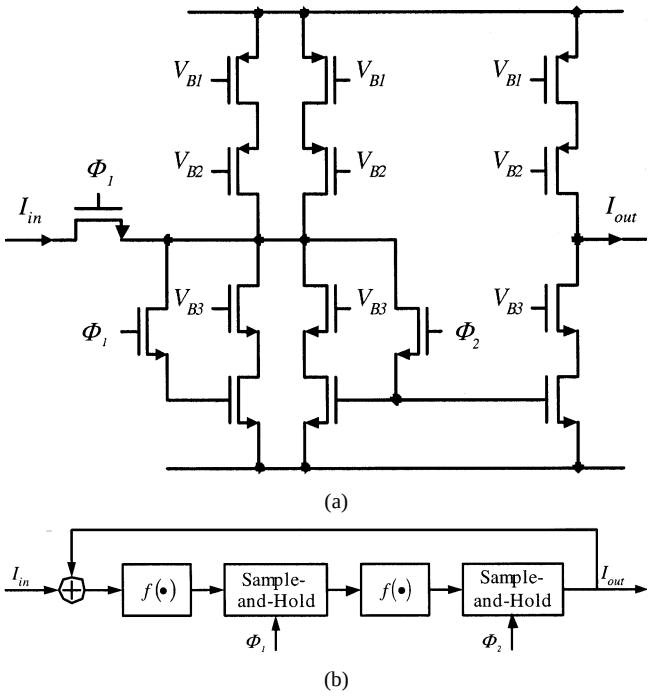

Fig. 18. A forward Eular integrator composed of two switched-current memory cells. (a) Circuit schematic for a forward Eular integrator. (b) Discrete-time system model for the forward Eular integrator.

D. Comparison With Conventional Wavelet Approximation

As described in Section III, the adaptive algorithm in the conventional wavelet approximation theory cannot regulate the modeling error distribution continuously. On the other hand, the nonlinear function $l = g(x)$ in the proposed companding approach is continuous and smooth so that it can modify the singularity of wavelet basis functions, and consequently the modeling error distribution, continuously. Therefore, while the adaptive algorithm is very useful in many other applications, the nonlinear companding technique is more efficient for analog circuit modeling, where continuous error distribution is required.

E. Application of Companding in Behavioral Modeling

The wavelet collocation method with nonlinear companding can be easily applied in analog circuit modeling. Taking advantage of the effectiveness of the nonlinear companding technique, we can equalize the relative modeling error at various input/output amplitudes by cutting the absolute modeling error at the small signal region and losing a little accuracy at the large signal region. The behavioral model generated by the wavelet collocation method can be incorporated into system level simulation tools, such as MATLAB SIMULINK, to verify the overall system performance. Note that, without those behavioral models, it is impossible to afford the verification of an entire analog/mixed-signal system containing a large number of components.

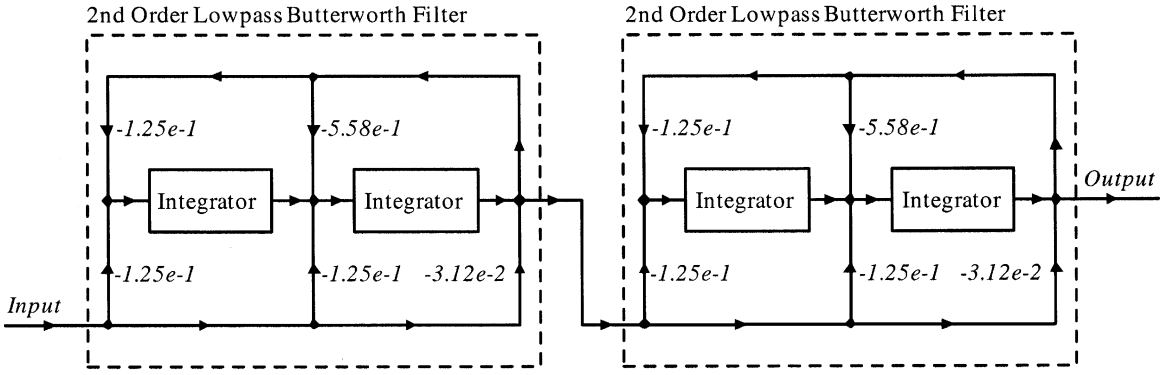

Fig. 19. Fourth-order lowpass Butterworth filter.

VI. Behavioral Modeling Examples

In this section, two circuit examples, a fourth-order switched-current filter and a VCO, are examined to demonstrate the effectiveness of the proposed wavelet collocation method in analog behavioral modeling.

A. Switched-Current Filter

In the past one decade, switched-current technique [25] has been considered as a promising technique for the monolithic implementation of mixed analog and digital VLSI. Due to the high-speed switching behaviors, general purpose circuit simulators such as SPICE always consume a large amount of computation time in simulating those switching networks. In recent years, the modeling and simulation methodology for switched-current circuits has also gained much attention [12]–[14]. In this subsection, we model the switched-current filter circuit by the proposed wavelet collocation method and compare it with other conventional approximation techniques.

1) Overview of Modeling Methodology: Fig. 1 shows the circuit schematic of a switched-current memory cell, which is the basic building block of switched-current circuits. Combining two memory cells, a forward Eular integrator is obtained in Fig. 18. In addition, a fourth-order lowpass Butterworth filter, which consists of four forward Eular integrators, is illustrated in Fig. 19.

The input-output relation for the basic memory cell is modeled in (1) The nonlinear function $f(\bullet)$ shown in Fig. 2 is obtained by SPICE simulation. Now, we apply the nonlinear companding algorithm to equalize the relative error at various input/output amplitudes.

Step 1) *Specify the modeling requirements*. In the current application, the relative simulation error should be equalized. Such a linguistic specification can be mathematically expressed as an explicit merit function.

$$Q = \left(Err_R|_{\text{Input}=\pm 5\mu A}\right)^2 + \cdots + \left(Err_R|_{\text{Input}=\pm 50\mu A}\right)^2. \quad (31)$$

The notation $Err_R|_{\text{Input}=\pm i\mu A}$ represents the relative simulation error (defined in (3)), when the switched-current memory cell is stimulated by a sinusoidal input of amplitude $\pm i\mu A \quad (i = 5, 10, \ldots, 50)$. After merit function (31) is minimized, we have $Err_R|_{\text{Input}=\pm 5\ \mu\text{A}} = \cdots = Err_R|_{\text{Input}=\pm 50\ \mu\text{A}}$, so that the minimum and equalized relative error is obtained.

Step 2) *Build the prototype function*. Our goal is to equalize the relative simulation error. Therefore, when function $f(\bullet)$ in Fig. 2 is expanded by wavelets, the absolute approximation error near $x = 0\ \mu$A should be smaller than that near $x = \pm 50\ \mu$A. We build a companding function with the combination of concave and convex functions, which is similar to (30) Define the prototype function in interval $\left[-5 \times 10^{-5}, 5 \times 10^{-5}\right]$ as

$$l = g(x) = \frac{5 \times 10^{-5}}{\ln(1 + 5 \times 10^{-5} p)} \cdot \text{sign}(x) \cdot \ln(1 + p|x|) \quad (32)$$

where p is a parameter controlling the nonlinearity of the function and its value is to be determined by an optimization process in Step 3.

Step 3) *Refine the prototype function*. With merit function (31) and prototype function (32), we optimize parameter p by Golden Section Search method [27]. As long as the minimum value of (31) is reached, the optimal p is found and consequently the proper companding function $l = g(x)$ is determined.

Function $f(\bullet)$ is thus mathematically represented by the wavelet expansion. The integrator, as shown in Fig. 18, is modeled by a discrete-time system including a number of static nonlinear functions $f(\bullet)$ and ideal sample-and-hold blocks. The fourth-order switched-current filter is behaviorally modeled by a signal flow graph in Fig. 19. Such a signal-flow-graph-based model is simulated by MATLAB SIMULINK to verify the accuracy of the proposed models.

2) Simulation Results of the Memory Cell: In this section, four methods are applied to approximate the nonlinear function $f(\bullet)$ in Fig. 2, which is very simple but helps us to make a full comparison between various approximation techniques. First, the polynomial and spline approximations are employed to express $f(\bullet)$ by 15 basis functions respectively. Second, we use the conventional wavelet collocation method with adaptive scheme to automatically select proper high-level wavelet basis functions so that the relative simulation error is equalized. As a result, 17 wavelet bases are chosen by the adaptive scheme to represent function $f(\bullet)$. Third, the wavelet collocation method

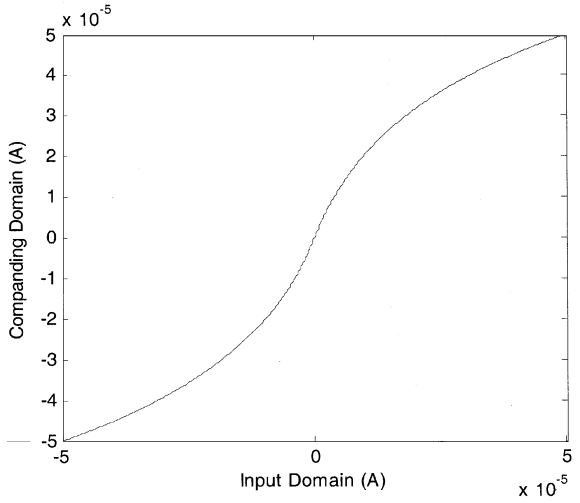

Fig. 20. Optimal nonlinear companding function $l = g(x)$ obtained by the optimization process.

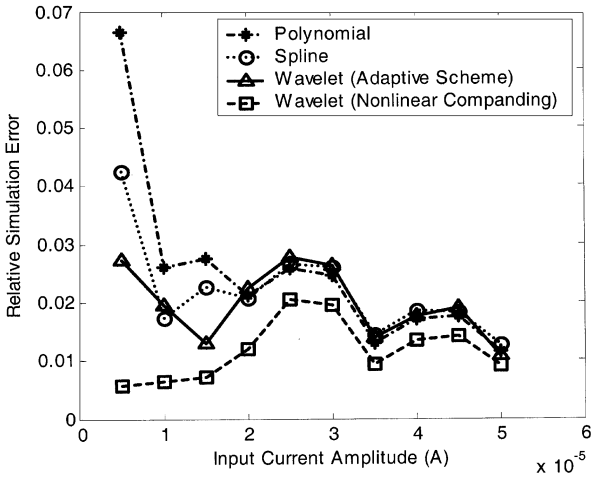

Fig. 21. Relative simulation error of different memory-cell models.

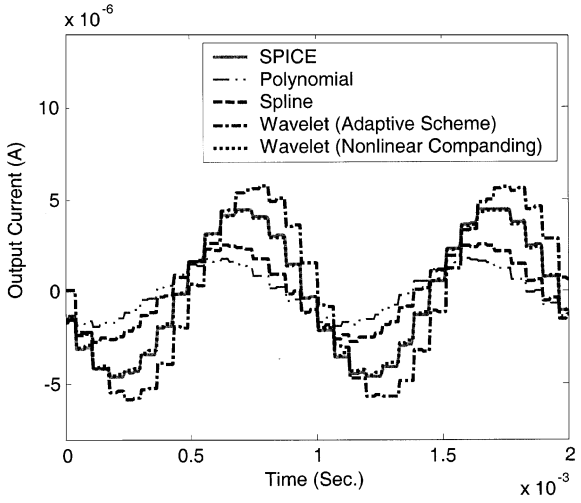

Fig. 22. Time domain response of the fourth-order switched-current filter.

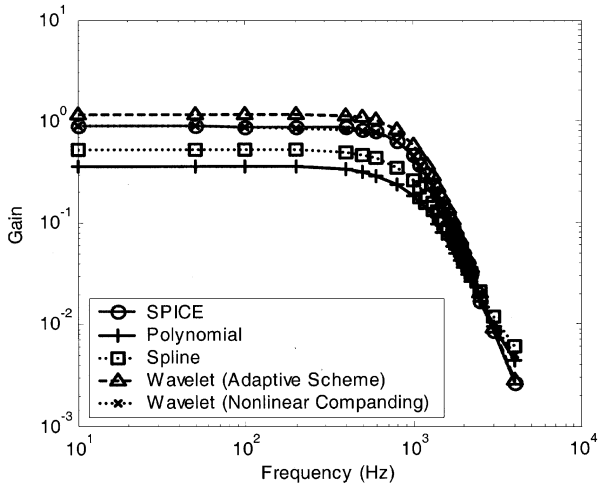

Fig. 23. Frequency domain response of the fourth-order switched-current filter.

with nonlinear companding is applied to approximate function $f(\bullet)$ by 15 basis functions. Fig. 20 depicts the optimal companding function $l = g(x)$, after the merit function (31) is minimized.

We test the developed behavioral models by transient simulations with various sinusoidal input amplitudes. Fig. 21 depicts the relative simulation error, defined in (3), for these models. Note that the relative error of both polynomial and spline model increases as the input current amplitude decreases, which implies that the modeling error distribution is completely uncontrolled. This observation is consistent with the simulation results listed in Table I. On the other hand, the wavelet expansion with either adaptive scheme or nonlinear companding is able to equalize the relative error at different input/output values. Moreover, it is shown in Fig. 21 that the modeling error of the nonlinear companding technique is less than that of the adaptive scheme, although the wavelet basis functions employed by the latter method are more than those employed by the former approach. From this point of view, the nonlinear companding method is more efficient than the conventional adaptive scheme in modeling switched-current circuits, which consists with the theoretical analysis in Section V-D.

3) Simulation Results of the Filter: Using the basic memory cell model developed above, we create the signal-flow-graph-based filter model in MATLAB SIMULINK. Such a discrete-time system model is then simulated by SIMULINK to verify the modeling accuracy of the entire filter.

a) *Time domain response*. First, we test the filter models by a sinusoidal input of frequency 1 kHz and amplitude $\pm 10\ \mu$A. Fig. 22 gives the time-domain simulation results obtained from SPICE and four kinds of different behavioral models. Again, these results indicate that the model developed by the wavelet collocation method with nonlinear companding is the most accurate one in predicting circuit behaviors.

b) *Frequency domain response*. Second, the filter model is tested with sinusoidal inputs of amplitude $\pm 10\ \mu$A at different frequencies. Fig. 23 depicts the frequency response obtained from SPICE and four kinds of different behavioral models. Note that the model expressed by wavelet

TABLE II
COMPUTATION COST FOR MODELING AND SIMULATING 4TH ORDER SWITCHED-CURRENT FILTER

Modeling/Simulation approach		Computation time (Sec.)
SPICE	Transient (SPICE) simulation in time domain $[0, 5ms]$	380
Wavelet model with nonlinear companding	SPICE simulation to compute $f(\bullet)$ at collocation points	39.6
	Optimize companding function & compute wavelet coefficients	22.6
	Transient (behavioral) simulation in time domain $[0, 5ms]$	2.8

expansion with nonlinear companding works much better than the other three ones.

c) *Simulation speed*. We build behavioral model and run behavioral simulation on a Pentium III-550 computer. Table II outlines the computation cost for both modeling and simulation. It is shown that SPICE simulation for such a switching filter is extremely expensive. On the other hand, the overall computation time for both behavioral model generation and behavioral simulation equals to $39.6 + 22.6 + 2.8 = 65$ seconds, which is less than 20% of the SPICE simulation time. In this example, the fourth-order switched-current filter is constructed by 8 identical memory cells. The behavioral model of the memory cell is extracted only once. Such a modeling procedure is not expensive, because the memory cell is a very small circuit block, as shown in Fig. 1. Then, the same memory cell models are repeatedly applied to build the entire filter model, which provides significant behavioral simulation speed-up. From this point of view, the benefit of generating behavioral models for basic circuit building blocks is clearly demonstrated.

B. Voltage-Controlled Oscillator (VCO)

VCOs are essential circuit components in phase-locked loops, which are basic analog building blocks used extensively in many analog and digital systems. Transistor-level simulation (e.g., by SPICE) of PLL circuit results in impractical run-times, because the acquisition procedure of a PLL circuit will take a large number of clock cycles [33]. In order to improve the simulation speed, it is necessary to extract the behavioral model for each component of the PLL circuit. Based on those behavioral models, high-level simulation can be executed efficiently to verify the overall PLL performance. In this part, we model the VCO by different wavelet collocation methods so that a full comparison can be made between the proposed nonlinear companding algorithm and those conventional wavelet approximation techniques.

1) Overview of Modeling Methodology: Fig. 24 shows the simplified model of a relaxation oscillator. The detailed implementation for the V–I converter block is depicted in Fig. 25, where $V_{\rm in}$ is the input voltage and $I_{\rm out}$ is the output current. If all components in Figs. 24 and 25 are ideal, the oscillation frequency is given by [33]

$$f_{\rm vco} = \frac{I_{\rm bias} - I_{\rm out}}{C_{\rm vco} \cdot V_{\rm Thres}} = \frac{1}{C_{\rm vco} \cdot V_{\rm Thres}} \cdot \left(I_{\rm bias} - \frac{V_{\rm in}}{R} \right). \quad (33)$$

However, the exact oscillation frequency does not comply with such a simple formulation, when nonideal behaviors are considered. For example, the relation between $f_{\rm vco}$ and will be

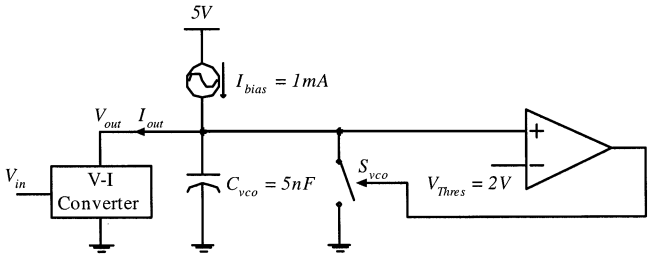

Fig. 24. A voltage-controlled oscillator (VCO).

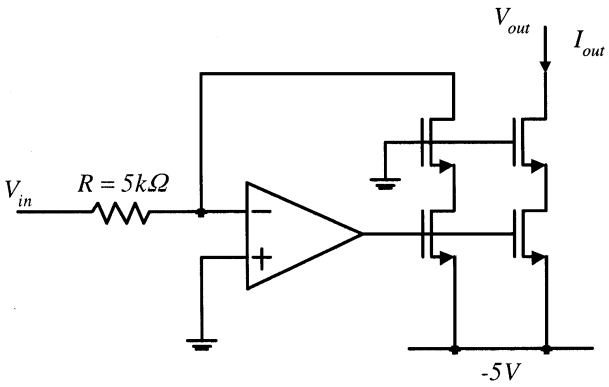

Fig. 25. Voltage–current converter in VCO.

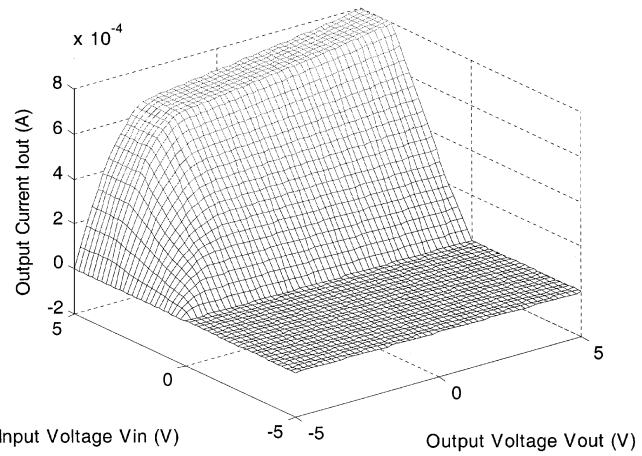

Fig. 26. Input–output relation for the V–I converter by SPICE.

nonlinear due to the nonlinear features of the operation amplifier and transistors in Fig. 25. In this example, we first expand the input–output relation of the V–I converter by wavelets. Then, we simulate the overall VCO in time domain to obtain its oscillation frequencies under different input voltages.

2) Modeling Errors in V–I Converter: The SPICE simulation result for various input voltage $V_{\rm in}$, output voltage $V_{\rm in}$ and output current $V_{\rm out}$ of the V–I converter is given in Fig. 26. It is shown that the output current $I_{\rm out}$ depends not only on the input voltage $I_{\rm out}$, but also on the output voltage $V_{\rm in}$ due to the finite

output impedance of the transistor. In the following, we illustrate how to construct the proper companding functions step by step to approximate the nonlinear function $I_{\rm out} = f(V_{\rm in}, V_{\rm out})$.

Step 1) *Specify the modeling requirements*. In this example, the relative simulation error $f_{\rm vco}$ should be equalized. Considering (33) one would find

$$\frac{df_{\rm vco}}{dI_{\rm out}} = \frac{-1}{C_{\rm vco}\cdot V_{\rm Thres}} \tag{34}$$

and

$$\frac{df_{\rm vco}}{\frac{I_{\rm bias}-I_{\rm out}}{C_{\rm vco}\cdot V_{\rm Thres}}} = -\frac{dI_{\rm out}}{I_{\rm bias}-I_{\rm out}} \tag{35}$$

$$\frac{df_{\rm vco}}{f_{\rm vco}} = \frac{d(I_{\rm bias}-I_{\rm out})}{I_{\rm bias}-I_{\rm out}}. \tag{36}$$

Equation (36) indicates that the relative simulation error of $f_{\rm vco}$ is actually determined by the relative error of the term $(I_{\rm bias}-I_{\rm out})$. Therefore, the modeling requirements are equivalent to equalizing the relative error of $(I_{\rm bias}-I_{\rm out})$. Such a linguistic specification can be mathematically expressed as an explicit merit function

$$Q = \sum_{i=1}^{N}\left(\frac{I_{\rm out}^i\big|_{\rm SPICE} - I_{\rm out}^i\big|_{\rm Model}}{I_{\rm bias}-I_{\rm out}^i\big|_{\rm SPICE}}\right)^2 \tag{37}$$

where N is the total number of collocation points $(V_{\rm in}^i, V_{\rm out}^i, I_{\rm out}^i)$, $I_{\rm out}|_{\rm SPICE}$ is the output current value obtained by SPICE and $I_{\rm out}|_{\rm Model}$ is the output current value evaluated by the developed behavioral model. After merit function (37) is minimized, the minimum and equalized relative error can be obtained.

Step 2) *Build the prototype functions*. Based on the requirements given in Step 1, our goal is to keep the relative simulation error of $(I_{\rm bias}-I_{\rm out})$ constant. As shown in Fig. 26, the value of $I_{\rm out}$ is monotonically increasing when $V_{\rm in}$ and $V_{\rm out}$ increase, and $I_{\rm out}$ reaches the maximum value $I_{\rm out} = 0.8$ mA when $V_{\rm in} = V_{\rm out} = 5$ V. Therefore, $(I_{\rm bias}-I_{\rm out}) = (1\text{ mA} - I_{\rm out})$ is reversely proportional to $V_{\rm in}$ and $V_{\rm out}$. In order to achieve constant relative error of $(I_{\rm bias}-I_{\rm out})$, we shall let the absolute error be reversely proportional to $V_{\rm in}$ and $V_{\rm out}$ too. It, in turn, means that the concave functions should be employed for nonlinear companding. Similar to the exponential function expressed in (28), we define two prototype functions in interval $[-5,\ 5]$ for companding $V_{\rm in}$ and $V_{\rm out}$ respectively.

$$l_{Vin} = g(V_{\rm in}) = \frac{10\cdot[\exp[p_{Vin}\cdot(V_{\rm in}+5)]-1]}{\exp(10p_{Vin})-1} - 5 \tag{38}$$

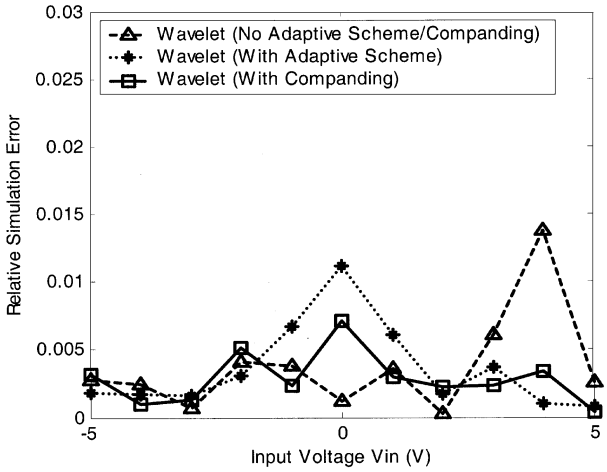

Fig. 27. Relative simulation error by three wavelet expansion methods.

$$l_{V\rm out} = g(V_{\rm out}) = \frac{10\cdot[\exp[p_{V\rm out}\cdot(V_{\rm out}+5)]-1]}{\exp(10p_{V\rm out})-1} - 5 \tag{39}$$

where $p_{V_{\rm in}}$ and $p_{V_{\rm out}}$ are two parameters controlling the nonlinearity of the functions and their values are to be optimized in Step 3.

Step 3) *Refine the prototype functions*. With merit function (37) and prototype functions (38). and (39) we optimize $p_{V_{\rm in}}$ and $p_{V_{\rm out}}$ by Levenberg-Marquardt method [27]. As long as the minimum value of (37) is reached, the optimal values of $p_{V_{\rm in}}$ and $p_{V_{\rm out}}$ are found and consequently the proper companding functions $l_{V_{\rm in}} = g(V_{\rm in})$ and $l_{V_{\rm out}} = g(V_{\rm out})$ are determined.

3) Simulation Results: Three wavelet collocation methods in all are applied to expand function $l_{V_{\rm out}} = g(V_{\rm out})$ of the V–I converter. First, the collocation method with neither adaptive scheme nor nonlinear companding is employed to express function $I_{\rm out} = f(V_{\rm in}, V_{\rm out})$ by 420 two-dimensional wavelet bases. Second, we use the conventional adaptive scheme to automatically select proper high-level wavelet basis functions in those regions where high accuracy is needed. As a result, 332 two-dimensional wavelet bases are chosen by the adaptive scheme to represent $I_{\rm out} = f(V_{\rm in}, V_{\rm out})$. Third, the nonlinear companding algorithm is applied to approximate $I_{\rm out} = f(V_{\rm in}, V_{\rm out})$ by 200 two-dimensional basis functions. The behavioral models developed by these three approaches are tested respectively. Fig. 27 depicts the relative error of oscillation frequency $f_{\rm vco}$ in correspondence with these three models.Table III outlines the computation time by SPICE and three behavioral models respectively, which is obtained on a Pentium III-550 computer. Several comments can be made according to the data in Fig. 27 and Table III.

a) When neither adaptive scheme nor nonlinear companding is applied, the maximum relative error of $f_{\rm vco}$ is about 1.4% associated with 420 wavelet basis functions. After the adaptive scheme is used, proper wavelet bases are automatically selected. As such, only the most important basis functions are picked up and the overall number of

TABLE III
COMPUTATION TIME FOR SIMULATING VOLTAGE-CONTROLLED OSCILLATOR IN TIME DOMAIN $[0, 200\ \mu s]$

V_{in} (V)	Computation time (Sec.)			
	SPICE	No adaptive scheme/companding	Adaptive scheme	Companding
-5	392	0.2635	1.1401	0.2345
-4	550	0.2546	1.1199	0.2285
-3	472	0.2522	1.0318	0.2467
-2	500	0.2609	0.9949	0.2247
-1	390	0.2376	1.0132	0.2325
0	432	0.2790	1.1697	0.2444
1	386	0.2254	0.8623	0.1941
2	364	0.1637	0.6252	0.1430
3	330	0.1129	0.4523	0.1001
4	329	0.0808	0.2942	0.0697
5	328	0.0794	0.3072	0.0687

wavelet bases is reduced without losing significant accuracy. It is shown in Fig. 27 that the adaptive scheme results in 332 basis functions, while the maximum relative error of f_{VCO} is reduced to 1.1%. Finally, using the nonlinear companding algorithm, the maximum relative error is further reduced to 0.8%, although the companding algorithm only employs 200 wavelet bases. The above comparison implies that the nonlinear companding algorithm is more effective than the conventional wavelet collocation techniques for this VCO example.

b) The computation time needed for behavioral simulation based on the generated models is much less than that for transistor-level simulation by SPICE. The total speed-up is more than two orders in time domain. In addition, due to the reduced number of wavelet bases, the behavioral simulation with nonlinear companding model is the most efficient one, even if the excessive phase for companding requires additional computation time[1].

VII. CONCLUSION

Efficient system-level simulation of analog/mixed-signal systems requires simple and accurate behavioral models for individual circuit components. The companding-oriented wavelet collocation method proposed in this paper is able to reduce the modeling errors and control the modeling error distribution continuously based on system-level simulation requirements. Moreover, the proposed companding scheme can efficiently reduce the number of base functions, i.e., the number of coefficients needed to represent the model. It, in turn, improves the simulation efficiency significantly at the system level. From this viewpoint, the wavelet collocation method exploits a new general-purpose approach for modeling analog circuits, as a counterpart of those conventional techniques.

On the other hand, we also notice two limitations of the proposed wavelet modeling approach. First, the nonlinear companding function is currently developed by a combination of manual design and automatic optimization. Second, the current model complexity will increase exponentially, if high-dimensional nonlinear functions are considered. Our future research work will focus on developing an automatic companding algorithm and extending the proposed modeling approach to high-dimensional function spaces. In addition, it is worth mentioning that the nonlinear companding method proposed in this paper can essentially be applied to any other basis functions with local support (e.g., radial basis functions). The detailed discussion on this issue will also be incorporated as a part of our future research.

[1]In our behavioral simulation program, the data structure for the behavioral model with adaptive scheme is more complicated than that for the other two models. For the wavelet model with adaptive scheme, additional information should be stored to identify those important wavelet basis functions which are automatically selected. Therefore, in Table III, the computation time for the model developed by adaptive algorithm is even larger than that for the model with neither adaptive scheme nor nonlinear companding, although the basis functions employed by the former model are less than those employed by the latter one.

REFERENCES

[1] L. T. Pillage and R. A. Rohrer, "Asymptotic waveform evaluation for timing analysis," *IEEE Trans. Computer-Aided Design*, vol. 9, pp. 352–366, Apr. 1990.

[2] P. Feldmann and R. W. Freund, "Efficient linear circuit analysis by padé approximation via lanczos process," *IEEE Trans. Computer-Aided Design*, vol. 14, pp. 639–649, May. 1995.

[3] L. Silveira, M. Kamon, I. Elfadel, and J. White, "A coordinate-transformed arnoldi algorithm for generating guaranteed stable reduced-order models of RLC circuit," *IEEE Int. Conf. on Computer Aided Design*, pp. 288–294, 1996.

[4] A. Odavasioglu, M. Celik, and L. T. Pileggi, "PRIMA: Passive reduced-order interconnect macromodeling algorithm," *IEEE Trans. Computer-Aided Design*, vol. 17, no. 8, pp. 645–654, Aug. 1998.

[5] J. Roychowdhury, "Reduced-order modeling of time-varying systems," *IEEE Trans. Circuits Syst. II*, vol. 46, pp. 1273–1288, Oct. 1999.

[6] J. Phillips, "Projection frameworks for model reduction of weakly nonlinear systems," in *IEEE Design Automation Conf.*, 2000, pp. 184–189.

[7] M. Rewienski and J. White, "A trajectory piecewise-linear approach to model order reduction and fast simulation of nonlinear circuits and micromachined devices," *IEEE Int. Conf. on Computer Aided Design*, pp. 252–257, 2001.

[8] J. Shao and R. Harjani, "Macromodeling of analog circuits for hierarchical circuit design," *IEEE Int. Conf. on Computer Aided Design*, pp. 656–663, 1994.

[9] R. Harjani and J. Shao, "Feasibility and performance region modeling of analog and digital circuits," *Analog Integr. Circuits and Signal Processing*, vol. 10, no. 2, pp. 23–43, June/July 1996.

[10] H. Liu, A. Singhee, R. Rutenbar, and L. R. Carley, "Rememberance of circuit past: macromodeling by data mining in large analog design spaces," in *IEEE Design Automation Conf.*, 2002, pp. 437–442.

[11] H. Unbehauen and G. Rao, *Identification of Continuous Systems*: Elsevier Science, 1987.

[12] E. Schneider and T. Fiez, "Simulation of switched-current systems," in *IEEE Int. Symp. on Circuits and Systems*, 1993, pp. 1420–1423.

[13] A. Yúfera and A. Rueda, "Studying the effects of mismatching and clock-feedthrough in switched-current filters using behavioral simulation," *IEEE Trans. Circuits Syst. II*, vol. 44, pp. 1058–1067, Dec. 1997.

[14] X. Zeng, W. Wang, J. L. Shi, P. S. Tang, and D. Zhou, "Analog behavioral modeling of switched current building block circuits," *Chinese J. Electron.*, vol. 10, no. 2, pp. 223–229, Apr. 2001.

[15] S. Mallat, "A theory for multiresolution signal decomposition: The wavelet representation," *IEEE Trans. Pattern Recog. Machine Intell.*, vol. 11, no. 7, pp. 674–693, Jul. 1989.

[16] I. Daubechies, *Ten Lectures on Wavelets*. Philadelphia, PA: SIAM, 1992.

[17] C. K. Chui, *An Introduction to Wavelets*. San Diego, New York: Academic Press, 1992.
[18] B. Alpert, "A class of bases in l2 for the sparse representation of integral operators," *SIAM J.Math. Anal.*, vol. 24, pp. 246–262, 1993.
[19] G. Beylkin, R. Coifman, and V. Rokhlin, "Fast wavelet transforms and numerical algorithms I," *Commun. Pure Appl. Math.*, vol. 44, pp. 141–183, 1991.
[20] G. Oberschmidt and A. Jacob, "Non-uniform wavelets on adapted grids for modeling edge singularities," in *Eur. Microwave Conf.*, Sept. 1997, pp. 1258–1263.
[21] D. Zhou and W. Cai, "A fast wavelet collocation method for high-speed circuit simulation," *IEEE Trans. Circuits Syst. I*, vol. 46, pp. 920–930, Aug. 1999.
[22] D. Zhou, W. Cai, and W. Zhang, "An adaptive wavelet method for nonlinear circuit simulation," *IEEE Trans. Circuits Syst. I*, vol. 46, pp. 931–938, Aug. 1999.
[23] X. Li, X. Zeng, D. Zhou, and X. Ling, "Behavioral modeling of analog circuits by wavelet collocation method," *IEEE Int. Conf. on Computer Aided Design*, pp. 65–69, Nov. 2001.
[24] W. Cai and J. Wang, "Adaptive multi-resolution collocation methods for initial boundary value problems of nonlinear PDE's," *SIAM J. Numer. Anal.*, vol. 33, no. 3, pp. 937–970, June 1996.
[25] J. Hughes, N. Bird, and I. Macbeth, "Switched current: A new technique for analogue sampled data signal processing," *IEEE Int. Symp. on Circuits and Systems*, pp. 1584–1587, 1989.
[26] R. Adams, *Sobolev Spaces*. New York: Academic, 1975.
[27] W. Press, B. Flannery, S. Teukolsky, and W. Vetterling, *Numerical Recipes in C The Art of Scientific Computing*. city, state/country?: Cambridge Univ. .
[28] H. Resnikoff and R. Wells, *Wavelet Analysis: The Scalable Structure of Information*. New York: Springer-Verlag, 1998.
[29] *Transmission Systems for Communications*. Winston-Salem, NC: Western Electric Co, 1970.
[30] D. Fisher, "Noise reduction system," in *Audio and HI-FI Handbook I*, R. Sinclair, Ed. Oxford, U.K.: Butterworth-Heinemann, 1993.
[31] Y. Tsividis, "Externally linear, time-invariant systems and their application to companding signal processors," *IEEE Trans. Circuits Syst. II*, vol. 44, pp. 65–85, Feb. 1997.
[32] D. Frey, "Exponential state space filters: A generic current mode design strategy," *IEEE Trans. Circuits Syst. I*, vol. 43, pp. 34–42, Jan. 1996.
[33] D. Johns and K. Martin, *Analog Integrated Circuit Design*. New York: Wiley, 1996.

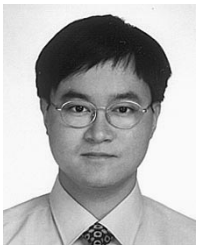

Xin Li received the B.S. and M.S. degrees in electronics engineering from Fudan University, Shanghai, China, in 1998 and 2001, respectively. He is currently working toward the Ph.D. degree at Carnegie Mellon University, Pittsburgh, PA.

His research interests include macromodeling and high-level simulation for RF/analog and mixed-signal systems.

Xuan Zeng (M'97) received the B.Sc. and Ph.D. degrees in electrical engineering from Fudan University, Shanghai, China, in 1991 and 1997, respectively.

She joined the Electrical Engineeering Department, Fudan University in 1997. Now she is a full professor and the Associate Head of Microelectronics Department at the same university. She was a visiting professor in the Electrical Engineeering Department, Texas A&M University, Dallas, in 2002. Her research interests include analog and mixed signal design automations (behavioral modeling, circuit simulation and analog layout generation), high speed interconnect analysis and design, current mode analog circuit design and ASIC design.

Dr. Zeng received the Cross-Century Outstanding Scholar Award from the Ministry of Education of China in 2002. She was the member of technical program committee of IEEE/ACM ASP-DAC in 2000. She is now the Panel Member of Information Science and Technology Committee of Shanghai China.

Dian Zhou received the B.S. degree in physics and the M.S. degree in electrical engineering from Fudan University, Shanghai, China, in 1982 and 1985, respectively. He received the Ph.D. degree in electrical and computer engineering from University of Illinois at Urbana-Champaign, in 1990.

He has been a full professor in Electrical and Computer Engineering Department, University of Texas at Dallas, since 1999. His research interests include high-speed VLSI systems, and CAD tools and algorithms.

Dr. Zhou received National Science Foundation (NSF) Research Initiation Award in 1991, IEEE Circuits and Systems Society Darlington Award in 1993, NSF Young Investigator Award in 1994, Chinese NSF Outstanding Overseas' Scientist Award in 1999, and was honored as Chinese Changjiang Scholar in 2002, respectively. He served as a panel member of the NSF CAREER Award in 1996. He was a Guest Editor for the *International Journal of Custom-Chip Design, Simulation and Testing*, and was an Associate Editor for IEEE TRANSACTIONS ON CIRCUITS AND SYSTEMS.

Xieting Ling graduated from the Physics Department of Fudan University, Shanghai, China, in 1958.

Since 1958, he has been with Fudan University and is now a Professor with the Electronic Engineering Department. In 1982, as the chairman, he was responsible for organizing the Electronic Engineering Department. He was a visiting research fellow with the Department of Electrical Engineering and Computer Science, University of California, Berkeley, in 1985, a visiting professor with the Engineering Faculty of Hiroshima University, Japan in 1986, and a visiting professor with the Department of Electrical and Electronic Engineering, Hong Kong University of Science and Technology, during 1992–1993. His research interests include computer-aided analysis and design, analog IC design, neural network, blind signal processing and application of chaos. He is the Editor of Acta Electronica Sinica, China and several other journals.

Prof. Ling has received the Improved Awards for Science and Technology by the State Education Commission of China and Government of Shanghai in 1986,1987, and 1999.

Wei Cai received the Ph.D. degree in applied mathematics from Brown University, Providence, RI in 1989.

He joined the Department of Mathematics, the University of North Carolina at Charlotte in 1989 as an assistant professor, later became an associate professor in 1995. In 1995, he joined the Department of Mathematics at the University of California at Santa Barbara as an Assistant Professor and later an Associate Professor. In 1996, he returned to the Department of Mathematics, the University of North Carolina at Charlotte and became a full Professor in 1999. His research interest includes numerical methods for model reduction, computational electromagnetics for parameter extraction for computer packaging and VLSI designs and photonic devices.